Electronic Supplementary Information

An Epidermal Wearable Microfluidic Patch for Simultaneous Sampling, Storage, and Analysis of Biofluids with Counterions Monitoring

Brince Paul Kunnel[ab*], and Silvia Demuru[a]

[a]Soft Transducers Laboratory, École Polytechnique Fédérale de Lausanne (EPFL) 2000 Neuchatel, Switzerland

[b]Micro and Nanosystems Centre, Tyndall National Institute, T12 R5CP Cork, Ireland

[*]Corresponding author, Email: brince.kunnel@tyndall.ie / brincepaul6@gmail.com

Materials and Methods

Materials

ETH 129 (calcium ionophore), sodium tetrakis[3,5-bis(trifluoromethyl)phenyl] borate (Na-TFPB), bis(2-ethylehexyl) sebacate (DOS), cyclohexanone, tetrahydrofuran, polyvinyl chloride (PVC), 2-nitrophenyl octyl ether (o-NPOE), tridodecylmethylammonium chloride (TDMACl), BUTVAR B-98 (PVB), poly(ethylene glycol)-block-poly(propylene glycol)- block-poly(ethylene glycol) (F127), agarose, pilocarpine, Phosphate-buffered saline (PBS) tablets, potassium chloride (KCl), sodium chloride (NaCl), calcium chloride ($CaCl_2$), glucose, urea, ammonium chloride (NH_4Cl), disodium hydrogen phosphate (Na_2HPO_4), hydrochloric acid (HCl), citric acid, monosodium phosphate (NaH_2PO_4), lactate, sodium bicarbonate($NaHCO_3$), sodium sulphate(Na_2SO_4), sodium nitrate($NaNO_3$), potassium thiocyanate(KSCN), and sodium hydroxide (NaOH) were purchased from Sigma Aldrich. Silver/silver chloride (Ag/AgCl) ink was purchased from DuPont, whereas carbon paste was obtained from Sun Chemical. All chemical products aforementioned were used without any further purification.

Preparation of membranes and gels

Ca^{2+} ion-selective membrane was prepared by dissolving 2 wt% ETH129, 1 wt% Na-TFPB, 130.9 wt% DOS, and 66 wt% PVC in 1320 µl THF,[49] whereas Cl^- selective membrane was prepared by dissolving 100 mg of 34:51:15 wt % ratio of PVC:o-NPOE: TDMACl in 1.0 mL THF.[60] To prepare the reference membrane, a 79.1 mg PVB, 50 mg NaCl, and 2 mg F127 were dissolved in 1 mL methanol using an ultrasonic bath until getting a homogenous mixture of membrane solution.[19,28,36] All the prepared membrane solutions were tightly sealed and stored at 4 °C until further use. Pilogel was prepared by dissolving 3% agarose in DI water at high temperature and adding 1% of pilocarpine with vigorous stirring for 1 min, whereas PBS gel was obtained by dissolving 3% agarose in PBS solution at high temperature. PBS solution was prepared by dissolving 1 PBS tablet in 200 mL DI water.

Sensors characterization and measurements

The sensitivity studies of Ca^{2+} sensors were conducted in $CaCl_2$ solution with varying concentrations of 0.25 mM to 2 mM, whereas Cl^- sensors sensitivity studies were evaluated in KCl solution with a concentration varying from 10 mM to 160 mM. The same concentration of $CaCl_2$ and KCl solutions was used to examine the repeatability and reproducibility of the fabricated Ca2+ and Cl^- sensors, respectively. The Ca^{2+} sensors selectivity studies were conducted by adding interfering ions' electrolytes such as 1 mM NH_4Cl, 100 µM glucose, 8 mM KCl, and 10 mM NaCl to 1mM $CaCl_2$ electrolytes. The Cl^- sensors selectivity studies were conducted by recording responses in different electrolytes of KCl, NH_4Cl, glucose, $CaCl_2$, and NaCl with maintaining 40 mM Cl^- concentration. The artificial ISF for Ca^{2+} sensors measurements consists of 3.48 mM KCl, 1.67 mM NaH_2PO_4, 107.7 mM NaCl, 5 mM NH_4Cl, and 5.5 mM glucose with varying 0.25 mM – 2 mM concentrations of $CaCl_2$ electrolytes, whereas the artificial sweat for Cl^- sensors measurements consists of 50 mM NaOH, 0.17 mM glucose, 8 mM urea, with a varying concentration of KCl from 10 mM to 160 mM.[36,63] Artificial ISF and sweat responses measurements were conducted by injecting different concentrations of the targeted electrolyte solution through a respective sensors compartment of SIFP using a commercial syringe pump (FLUIGENT) at ~5 µL/min constant flow rate. All the measurements were ceased for 30 seconds for each electrolyte concentration change. Interference tests to agonist agent were conducted by recording Ca^{2+} sensors Cl^- sensors responses with the addition of 1% pilocarpine in 1 mM $CaCl_2$ and 40 mM KCl, respectively. pH effect on Ca^{2+} sensors were evaluated by recording responses in 0.25 mM $CaCl_2$ (at pH 7 and pH8) and 2mM $CaCl_2$ (at pH 7 and pH8), whereas Cl^- sensors were examined at 40 mM KCl (at pH 7 and pH8) and 160 mM KCl (at pH 7 and pH8). The temperature depends on Ca^{2+} sensors and Cl^- sensors were conducted by recording responses in $CaCl_2$ (in 0.25mM and 2 mM concentration) and KCl (in 10mM and 160 mM concentration), respectively at 25°C and 40 °C temperature. The selectivity coefficient of the Ca^{2+} sensor and Cl^- sensors to various ions was estimated using a separate solution method. For mechanical stability evaluation, the fabricated sensors adhered to different radius curved PMMA surfaces (70 mm, 60mm, and 40mm curved radius) fabricated via laser cutting and corresponding responses (resistance variation at different strain and signals in respective sensors electrolytes) were recorded. The signal stability of the skin interfaced patch was evaluated by well-fixing the SIFP (without integration of the storage module) to the subject wrist and filling Ca^{2+} sensor and Cl^- sensor compartments with 1 mM $CaCl_2$ and 40 mM KCl, respectively, followed by recording sensor's responses while subject undergoing various activities. The SIFP's inlets and outlets were tightly closed to avoid any evaporation of electrolytes during measurements. The acceleration during different activities was recorded by attaching a smartphone having an accelerometer to the subject's forearm. The ion chromatography measurement was executed using ProfIC Vario 15 Cation (Metrohm) at room temperature. The samples were diluted (1:100 ratio) with 18 MΩ ultrapure water (Milli-Q, Millipore, Billerica).

SIFP interfacing circuit and signal processing

The circuit for SIFP interfacing followed the same as our previously reported work except for a slight change in software programming to increase the data acquisition interval.[36] In brief, a low power AD 8608 (operating current: 1mA, Analog Devices) based four-channel amplifier was used to design the separate high impedance voltage buffers for the signal acquisitions from Ca^{2+} and Cl^- sensor. Each sensor's signal conditioning path followed the low pass filter with a cut-off frequency of 14.5 Hz, which eliminates high-frequency noise. A separate biasing circuit fixed the PVB reference electrode's potential with respect to the Ca^{2+} and Cl^- ion-selective sensor, which ensured the positive signals acquisition from the ion-sensors. The conditioned signals from Ca^{2+} and Cl^- sensors were fed to the microcontroller board through an inbuilt 12 bit ADC. A low-power SAMD 21 based MCU (1.62V minimum operating voltage) platform consists of 32KB SRAM memory and integrated with stand-alone multi-radio modules (NINA-W10) was used for data processing and transmission. The Arduino development environment was used for the programming to process the data. The stimulation module circuit consists of the booster with a V/I converter to deliver a constant current of 1.3 mA to the anode and cathode. The stimulation module was coupled to the main PCB through a single pole double throw (SPDT) sliding switch, which selects the stimulation/sensing module and avoided simultaneous operation of both. A single 3.7 V lithium-ion battery achieved the power delivery to both the sensing and stimulation module. The processed sensors data were wirelessly transmitted to a smartphone, and an android based application facilitates numerical and graphical visualization of the sensors reading. The system interface also enabled the cloud storage of the sensors reading, which was retrieved for further analysis.

On-Body SIFP Biofluid Analysis Procedure

On-body evaluation of the developed SIFP was carried out in compliance with the protocol approved by the EPFL Human Research Ethics Committee (HREC No. 081-2020 / 24.11.2020). The volunteer wrist was wiped with an alcohol swab before attaching SIFP. The patches were precalibrated with a two-point calibration method in a lower and higher concentration of standard electrolyte solution of respective ion sensors before mounting on the body. This calibration enabled the conversion of the acquired ion sensors reading to respective ion concentrations after the measurement. For the measurement, first, the

iontophoretic stimulation module was activated for 10 min to generate sweat and ISF. The sensors readings were recorded after filling the respective biofluid's storage module and further stopping the fluids flow. Each measurement lasted for 45 min. After the measurement, the patches were post-calibrated with a similar method based on two-point calibration to extract accurate readings. In a hydration condition study, the volunteer took food and fluids before 40 minutes of the experiments whereas, the dehydration study was performed after 4 hours of fasting to obtain mild dehydration.

Figures

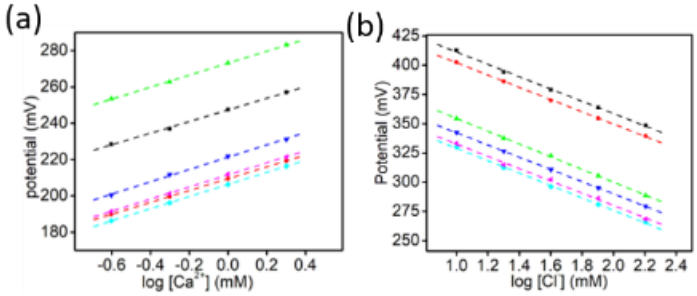

Fig. S1. Reproducibility study of the SIFP's (a) Ca^{2+} and (b) Cl^- ion-selective sensors. The sensors were fabricated under similar conditions and tested in their respective electrolyte solutions with varying concentrations of 0.25-2mM for $Ca^{2+}$and 10-160 mM for Cl^-. The variations in the absolute potential can be resolved by a baseline correction after the sensors' calibration.

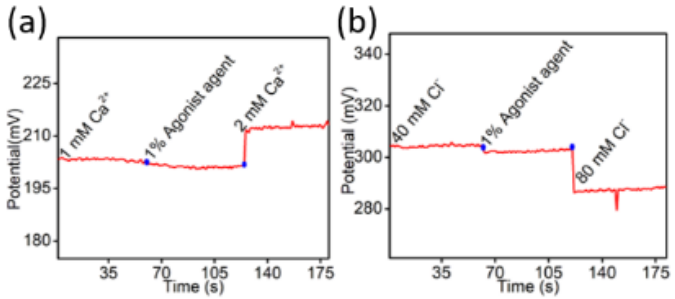

Fig. S2. Response of the SIFP's (a) Ca^{2+} and (b) Cl^- ion-selective sensors towards 1% agonist agent as an interfering substance. This study shows that the agonist agent has negligible interference to each sensor response.

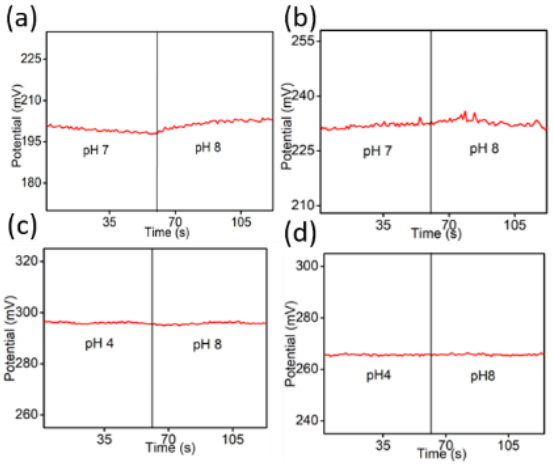

Fig. S3. Response of the SIFP's Ca^{2+} ion-selective sensors at pH 7 and at pH 8 (a) in 0.25 mM and (b) in 2 mM concentration of Ca^{2+} ion, and Cl^- ion-selective sensors at pH 4 and at pH 8 (c) in 40 mM and (d) in 160 mM concentration of Cl^- ion.

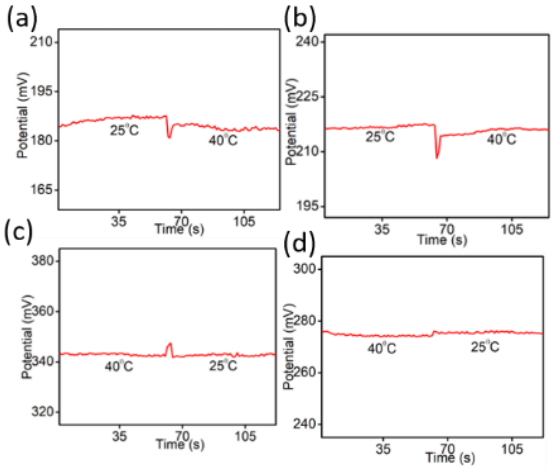

Fig. S4. Temperature influence study of SIFP's Ca^{2+} ion-selective sensors (a) with 0.25 mM and (b) with 2 mM concentration of Ca^{2+} ion, and Cl^- ion-selective sensors (c) with 40 mM and (d) with 160 mM concentration of Cl^- ion at 25°C and at 40°C.

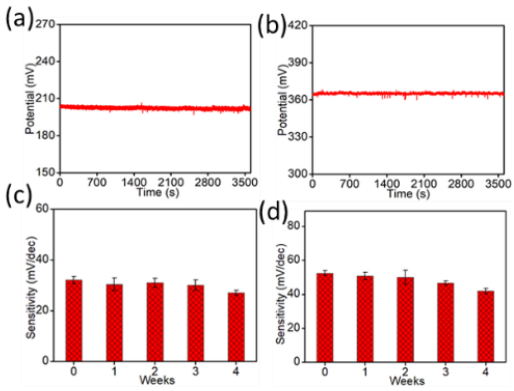

Fig. S5. Long term stability analysis of the SIFP's (a) Ca^{2+} and (b) Cl^- ion-selective sensors. Four-week storage stability analysis of the SIFP's (c) Ca^{2+} and (d) Cl^- ion-selective sensors. (The error bar indicates a standard error, n=3).

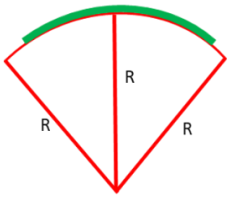

Fig. S6. Schematic illustration of the mechanical bending stability evaluation experiments. The fabricated sensors (green colour surface) adhered to the different radius (R) curved PMMA surfaces to evaluate the changes in electrical parameters.

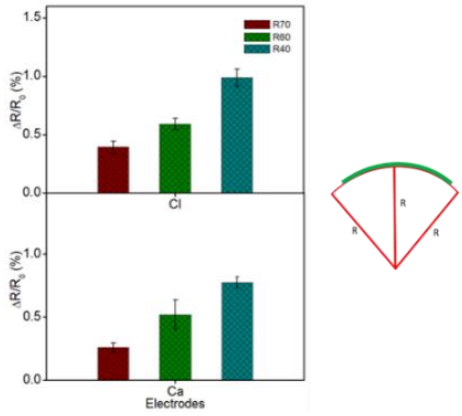

Fig. S7. Mechanical deformation analysis of SIFP's sensors. Percentage change in resistance of SIFP's Ca^{2+} (top) and Cl^- (bottom) ion-selective sensors during 70 mm, 60 mm, and 40 mm radius (R) bending state (R_0 represents initial ion-selective sensors resistance and ΔR represents a change in resistance of ion-selective sensors during bending state). (The error bar indicates a standard error, n=5).

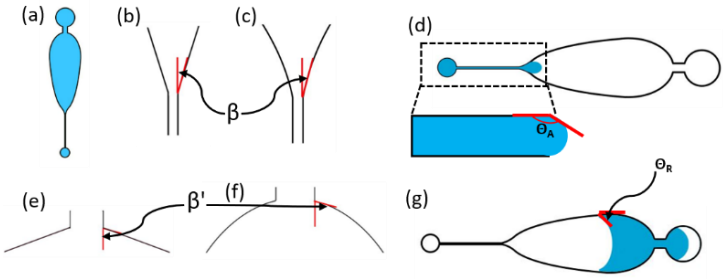

Fig. S8. (a) Schematic illustration of the fabricated SIFP transport module with fluid flow. Illustration of the inlet channel divergent joint to sensing chamber with (b) straight connection with angle β and (c) divergent connection with angle β used for optimizing the inlet shape. (d) Illustration of the fluid transport from the inlet channel to sensing chamber. The fluid interface advances along the diverging wall when Θ_A+ β >180°, where Θ_A is the critical advancing contact angle at which the contact line starts to move. Illustration of the outlet channel convergent joint from sensing chamber with (e) straight connection with angle β', and (f) divergent connection, and the angle β' used for optimizing the outlet shape. (g) Illustration of the fluid flow from the sensing chamber to the outlet of the transport module. Here, the fluid has both the advancing (towards outlet) and receding (from the chamber) fronts. When the contact angle is less than the receding contact angle Θ_R, the fluids rear meniscus begins to recede.

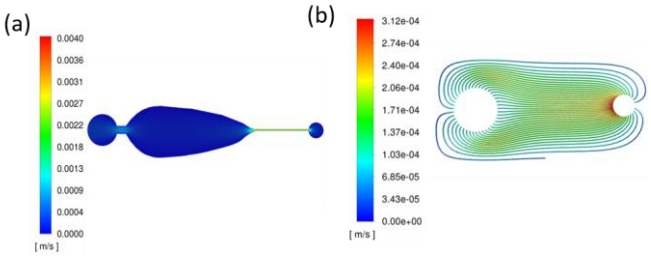

Fig. S9. Optimization of the SIFP fluidics. (a) SIFP transport module's velocity counter lines plot and (b) SIFP storage module's velocity path line distribution

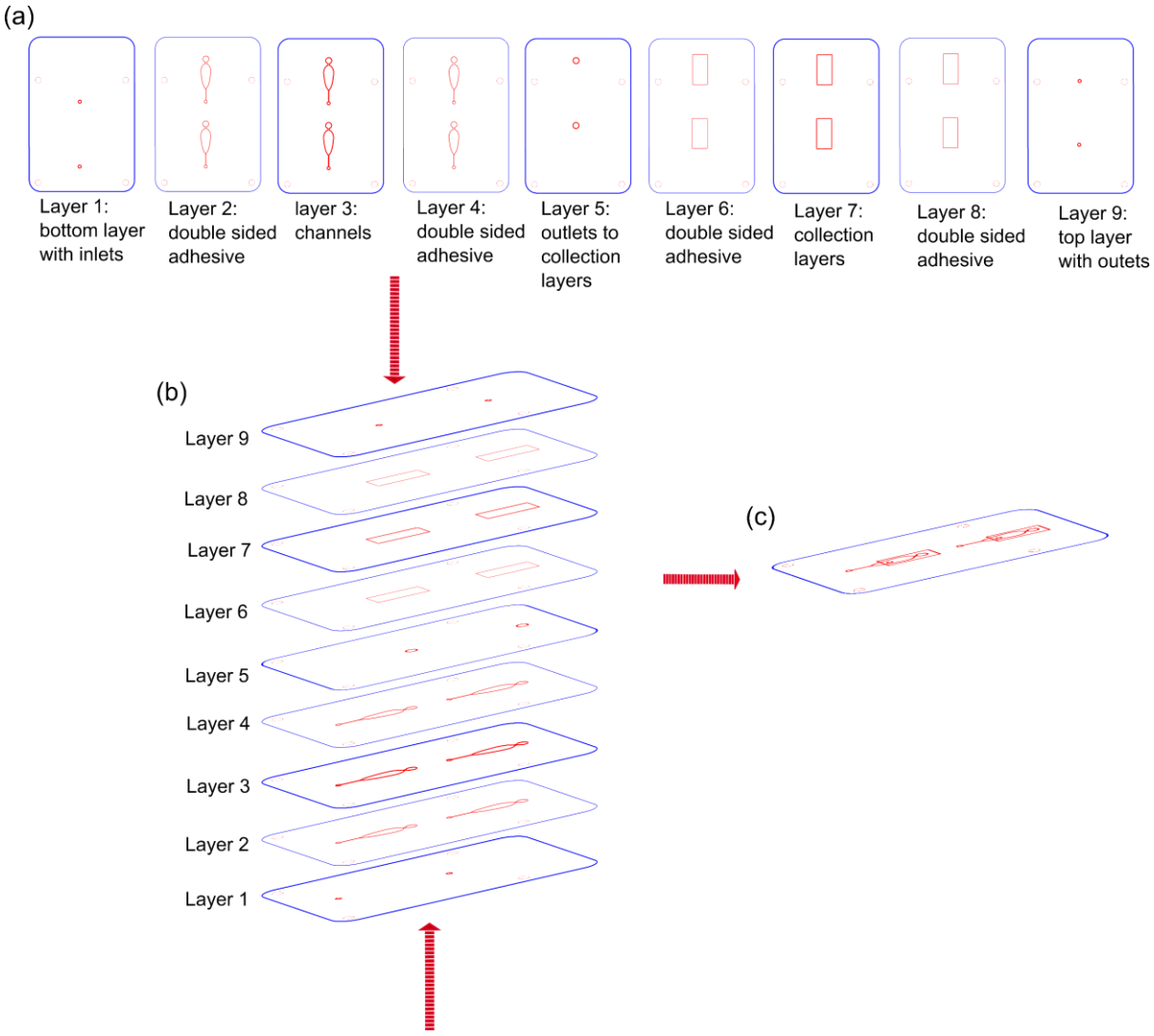

Fig. S10. Schematic illustration of the SIFP fluidics fabrication. (a) CAD design of each layer of the SIFP fluidics used for patterning. (b) Vertical stacking of the patterned layers in a sequential way generates the SIFP fluidics. (c) Illustration of the SIFP fluidics obtained after stacking of pattered layers.

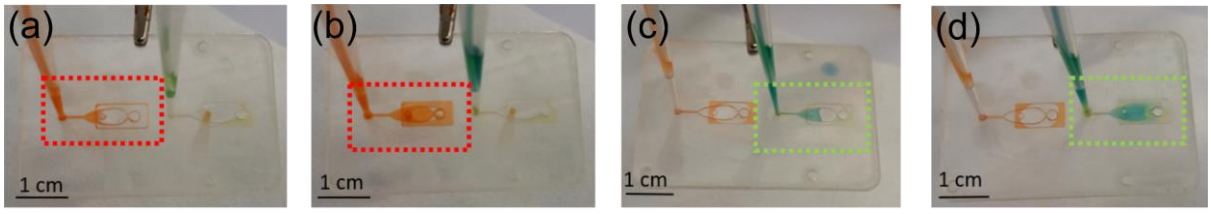

Fig. S11. Optical images of SIFP fluidics leakage test (a) fluid flow through transport module and (b) filling the storage module of ISF compartment, (c) fluid flow through transport module and (d) filling the storage module of sweat compartment.

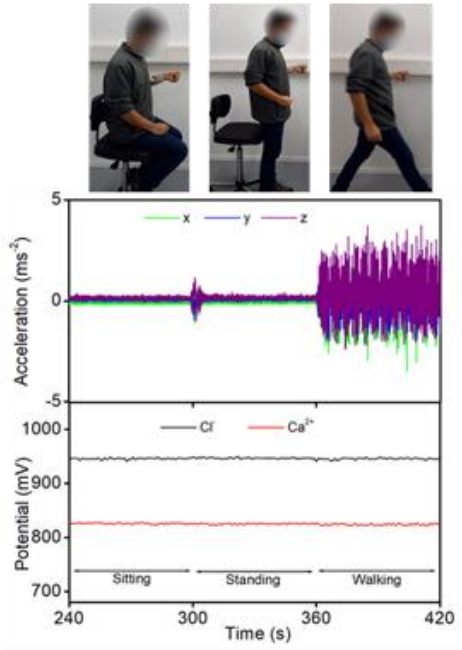

Fig. S12. Illustration of stability of SIFP's ion-selective sensors during sitting, standing, and slow walking activities (the monitored acceleration profile during the activities are depicted at the top).

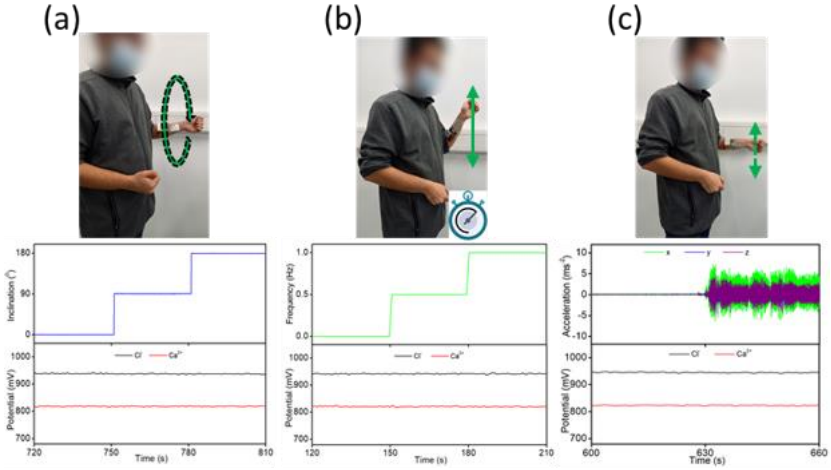

Fig. S13. Evaluation of the stability of SIFP sensor's responses during the interfacing with the skin with (a) wrist rotation: the SIFP's ion-selective sensors responses and corresponding angle of inclination are presented; (b) forearm waving: the SIFP's ion-selective sensors responses and corresponding frequency of waving are presented; (c) forearm vibration: the SIFP's ion-selective sensors responses and corresponding acceleration profile recorded during arm vibration are presented.

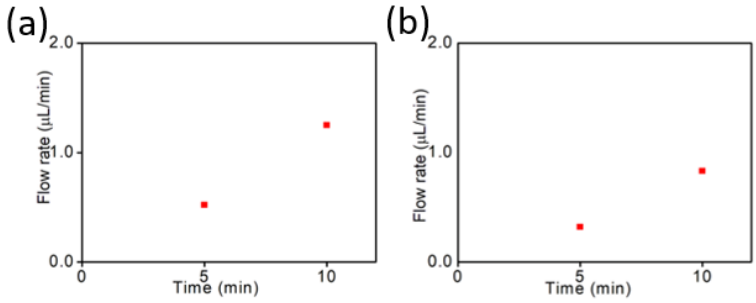

Fig. S14. Optimization of stimulation duration for adequate sampling of biofluids. The flow rate study was performed by controlling sweat secretion rate by activating the stimulation module for a duration of a 5 min and then 10 min and the corresponding flow rate was calculated based on the total volume of the transport module of the SIFP and the total time taken by the biofluids to reach their respective transport module's outlet.

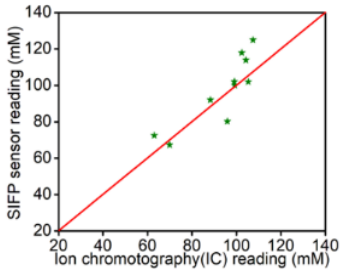

Fig. S15. The reliability of the developed SIFP for biofluid analysis is demonstrated by showing a correlation between one of the SIFP ion-selective sensor's (Cl^-) sweat concentration profiles with ion-chromatographic measurements.

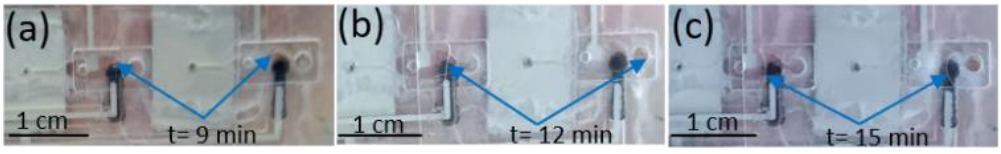

Fig. S16. On-body biofluid analysis during dehydration state. (a-c) optical images of the flow dynamics of the secreted ISF and sweat through respective ISF and sweat compartment's transport module and storage module of the SIFP (fluids advancing fronts at various times is indicated).

Tables

Table S1. Logarithmic selectivity coefficients for SIFP's Ca^{2+} and Cl^- ion-selective sensors to various ions.

$logK_{i,j}^{pot}$	Coefficients value
$logK_{Ca,K^+}^{pot}$	-2.8
$logK_{Ca,Na^+}^{pot}$	-3.4
$logK_{Ca,NH_4^+}^{pot}$	-3.5
$logK_{Cl,Lactate^-}^{pot}$	-5.3
$logK_{Cl,NO_3^-}^{pot}$	-2.8
$logK_{Cl,SO_4^{2-}}^{pot}$	-6.6
$logK_{Cl,HCO_3^-}^{pot}$	-1.0
$logK_{Cl,HPO_4^{2-}}^{pot}$	+0.7
$logK_{Cl,SCN^-}^{pot}$	-3.6

Table S2. Optimization in the selection of gels for adequate biofluid flow through the channel for the analysis.

Anode	Cathode	Sufficient sweat flow in fluidics	Sufficient ISF flow in fluidics
PBS gel	PBS gel	No	No
PBS gel	Pilo gel	No	No
Pilogel	PBS gel	Yes	Yes